CrystEngComm

Accepted Manuscript

ROYAL SOCIETY OF CHEMISTRY

www.rsc.org/crystengcomm

Graphical contents entry

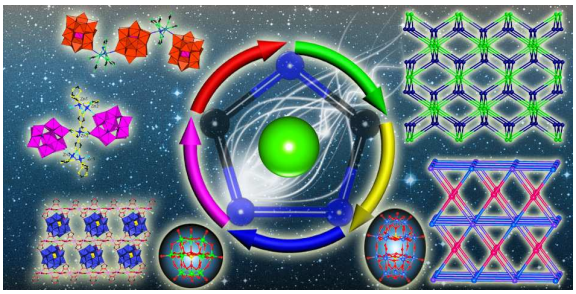

A family of organic–inorganic hybrid materials built by Keggin/Wells-Dawson polyoxometalate with metal–1,2,4-triazole units has been synthesized through modulating the pH value.

Cite this: DOI: 10.1039/c0xx00000x

www.rsc.org/xxxxxx

ARTICLE TYPE

Assembly of Organic−Inorganic Hybrid Materials Constructed from Polyoxometalate and Metal–1,2,4-triazole units: Synthesis, Structures, Magnetic, Electrochemical and Photocatalysis Properties

Yan-Qing Jiao, Chao Qin,* Hong-Ying Zang, Wei-Chao Chen, Chun-Gang Wang, Tian-Tian Zheng, Kui-Zhan Shao, Zhong-Min Su*

Received (in XXX, XXX) Xth XXXXXXXXX 20XX, Accepted Xth XXXXXXXXX 20XX
DOI: 10.1039/b000000x

A series of organic−inorganic hybrid compounds built by Keggin and Wells-Dawson polyometalates with TM-trz complexes (Htrz=1,2,4-triazole) were obtained at different pH values under hydrothermal conditions, namely, $[Co_2(H_2O)_2(Htrz)_5][SiW_{12}O_{40}]\cdot 2.5H_2O$ (**1**), $[Zn_5(Htrz)_8(trz)_2(H_2O)_8][SiW_{12}O_{40}]_2\cdot 10H_2O$ (**2**), $[Cu^{I}_2Cu^{II}_4(Htrz)_4(trz)_4Cl_2][GeW_{12}O_{40}]\cdot 15H_2O$ (**3**), $[Cu^{I}_2Cu^{II}_4(Htrz)_4(trz)_4Cl_2][SiW_{12}O_{40}]\cdot 15H_2O$ (**4**), $K_2Na_2(H_2O)_2[Co_{11}(trz)_{14}(H_2O)_{14}][P_2W_{18}O_{62}]_2\cdot 29H_2O$ (**5**) and $[Cu_{12}(trz)_{10}(Htrz)_2(OH)_4(SO_4)_2(H_2O)_6][P_2W_{18}O_{62}]\cdot 28H_2O$ (**6**). All the compounds were characterized by single-crystal X-ray diffractions, TG analyses and powder X-ray diffractions. Compound **1** contains a kind of bimetal-organic segment $[Co_2(Htrz)_5]^{4+}$, which could be regarded as a quasi-sinusoid-like chain. **2** is a dimer constructed from two $[SiW_{12}O_{40}]^{4-}$ linked by $[Zn_5(trz)_2(Htrz)_8]^{8+}$ motif. In **3** and **4**, the 2D wall-like layer constructed by the Cu(II) ions and Htrz ligands are extended into 3D frameworks by polyanions. **5** shows a complicated three-dimensional (3D) framework with a $\{4^{12}\cdot 6^{12}\cdot 8^4\}\{4^6\}_2$ topology. Compound **6** is also a complicated 3D structure based on the triangular trinuclear Cu-trz unit and $[P_2W_{18}O_{62}]$ polyanions. To the best of our knowledge, **6** represents the maximum copper cluster linked by amine in the POMs system. The structural diversities reveal that the pH value of the reaction system plays a crucial role in the assembly of POM-base hybrids. Moreover, the optical band gaps, the electrochemical properties, the magnetic properties and the photocatalytic properties of the compounds have been investigated.

Introduction

Polyoxometalates (POMs), famous as an intriguing and distinctive class of inorganic metal–oxygen clusters, have become one of the most varied growing areas in inorganic chemistry and merited enduring attention not only because of their compositional diversity and structural versatility but also owing to their promising applications in the fields of catalysis, magnetism, electrochemistry, photochemistry, and medicine.[1–2] However, POMs as inorganic crystalline materials have their own disadvantages in compatibility and processability, which hinder the further engineering of POMs into multifunctional materials. As a consequence, the design and assembly of novel POMs-based organic−inorganic hybrids with charming structures and 'value-adding' properties has been an attractive and challenging mission in POM chemistry.[3]

To date, a multitude of POMs-based hybrids have been reported, however, examples of high dimensional POM-supported hybrids, especially with polynuclear metal clusters are still relatively rare. Currently, the largest copper cluster linked by organic amine ligands in POM-based hybrids is the nonanuclear subunit from $\{Cu_9(2\text{-ptz})_{12}(H_2O)_6(PMo_{12}O_{40})_2\}\cdot H_2O$.[4] In this regard, the judicious choice of appropriate organic ligands is extremely important in the self-assembly process of prospective POMs-based multinuclear clusters seeing that organic ligands may control and adjust the topologies of metal-organic frameworks (MOFs).[5] Generally, N-donor organic ligands with the smaller steric hindrance, the more donor atoms, the flexible coordination sites and the good fitting of the coordination environment of metal ions and POMs are beneficial for the construction of POM-supported hybrids containing polynuclear metal complexes. In light of this, the unsubstituted 1-H-1,2,4-triazole (abbreviated to 'trz') has captured our attention because of its strong and typical coordination capacity for bridging metal ions to result in polynuclear clusters with unusual structural diversity, which combines the coordination mode of both imidazoles and pyrazoles to provide more potential coordination sites.[6] Besides, the metal–triazole polynuclear clusters have been used as secondary building units to construct stable and high-dimensional MOFs.[7] Notwithstanding, 1,2,4-triazole has not been widely employed in the POMs-based inorganic−organic system, due to its inherent deficiency, such as its very short bridging length and the ease of forming highly insoluble and intractable products, which is difficult to curb and control at the molecular

level.[8] However, Lu *et al.* finally made important breakthrough in 2010, in which trz ligands played the supportive role in the polycatenane compound $\{Ag_{26}(trz)_{20}\}[PW_{12}O_{40}]_2$ containing the adamantine-like $\{Ag_{24}(trz)_{18}\}^{6+}$ nanocage.[9] Subsequently, a novel metal-organic *pseudo*rotaxane framework $Ag_{14}(trz)_{10}[SiW_{12}O_{40}]$ and POMs-based supramolecular aggregate $Ag_{10}(Htrz)_2(trz)_6[SiW_{12}O_{40}]_2$ were discovered.[10]

In view of the prominent work of the above mentioned, recently we have thus initiated a study on the reaction of 1,2,4-triazole and transition metals in the presence of the classical Keggin/Wells-Dawson POMs. Herein, a series of novel POM-based inorganic–organic hybrids, namely, $[Co_2(H_2O)_2(Htrz)_5][SiW_{12}O_{40}]\cdot 2.5H_2O$ (**1**), $[Zn_5(Htrz)_8(trz)_2(H_2O)_8][SiW_{12}O_{40}]_2\cdot 10H_2O$ (**2**), $[Cu^I_2Cu^{II}_4(Htrz)_4(trz)_4Cl_2][GeW_{12}O_{40}]\cdot 15H_2O$ (**3**), $[Cu^I_2Cu^{II}_4(Htrz)_4(trz)_4Cl_2][SiW_{12}O_{40}]\cdot 15H_2O$ (**4**), $K_2Na_2(H_2O)_2[Co_{11}(trz)_{14}(H_2O)_{14}][P_2W_{18}O_{62}]_2\cdot 29H_2O$ (**5**) and $[Cu_{12}(trz)_{10}(Htrz)_2(OH)_4(SO_4)_2(H_2O)_6][P_2W_{18}O_{62}]\cdot 28H_2O$ (**6**), have been successfully obtained under hydrothermal conditions. Compounds **3** and **4** are isostructural three-dimensional frameworks, which are constructed from the $Cu^{I/II}$–organic sheets and polyanions, possessing two-directional intersecting channels with window dimensions of 9.4 × 5.5 $Å^2$ along *a* axis and 8.9 × 6.8 $Å^2$ along *b* axis, respectively. It is noteworthy that compound **5** contains the largest-ever number of cobalt ions in the $\{P_2W_{18}\}$-based inorganic–organic hybrids. One structural feature of **6** is that there exist a triangular trinuclear Cu-trz unit-based motif, in which SO_4^{2-} anion as the connector provides a great benefit for aggregating the Cu_3-triads into the larger moieties and further generating the novel 3D framework. To the best of our knowledge, **6** represents the maximum copper cluster in the POMs system. The optical band gaps, the electrochemical properties and the magnetic properties have also been investigated in detail. Besides, compounds **5**–**6** are employed as the heterogeneous catalysts for photocatalytic degradation of methylene blue (MB), giving fairly high catalytic activity, which provides impetus for further development of photocatalysts from other inorganic–organic hybrid materials based on multinuclear subunits and polyoxometalates.

Experimental

Synthesis

$K_6[\alpha\text{-}P_2W_{18}O_{62}]\cdot 15H_2O$, $K_8[\gamma\text{-}GeW_{10}O_{36}]\cdot 6H_2O$, and $K_8[\gamma\text{-}SiW_{10}O_{36}]\cdot 12H_2O$ were synthesized according to the literature and characterized by IR spectra.[11] All the other reagents were used as purchased without further purification.

$[Co_2(H_2O)_2(Htrz)_5][SiW_{12}O_{40}]\cdot 2.5H_2O$ (1).

A mixture of $H_4[SiW_{12}O_{40}]$ (0.496 g, 0.2 mmol), 1,2,4-triazole (0.069 g, 1.0 mmol) and $CoCl_2\cdot 6H_2O$ (0.237 g, 1.0 mmol) was dissolved in 8.0 mL of distilled water. The pH value of the mixture was carefully adjusted with 2 M HCl solution to approximately 1.96 and then sealed into a 15 mL Teflon-lined autoclave and heated at 180 ºC for 3 days and then cooled down to room temperature at a rate of 10 ºC h^{-1}. Pink crystals of **1** were collected and washed with distilled water and dried in air to give the product (yield: 35 % based on Co). Elemental analysis calcd. (%) for $C_{10}H_{24}N_{15}O_{44.5}Co_2SiW_{12}$: C 3.51, H 0.71, N 6.15, Si 0.82, Co 3.45, W 64.54; found: C 2.99, H 1.21, N 6.78, Si 0.59, Co 3.87, W 65.23. IR (cm^{-1}): 3435 (s), 1629 (m), 1558 (w), 1422 (m), 1150 (w), 1085 (m), 936 (w), 801 (m), 671 (m).

$[Zn_5(Htrz)_8(trz)_2(H_2O)_8][SiW_{12}O_{40}]_2\cdot 10H_2O$ (2).

A mixture of $H_4[SiW_{12}O_{40}]$ (0.496 g, 0.2 mmol), 1,2,4-triazole (0.069 g, 1.0 mmol) and $Zn(CH_3COO)_2\cdot 2H_2O$ (0.219 g, 1.0 mmol) was dissolved in 8.0 mL of distilled water. The pH value of the mixture was carefully adjusted with 2 M HCl solution to approximately 3.30 and then sealed into a 15 mL Teflon-lined autoclave and heated at 180 ºC for 3 days and then cooled down to room temperature at a rate of 10 ºC h^{-1}. Colorless crystals of **2** were collected and washed with distilled water and dried in air to give the product (yield: 33 % based on Zn). Elemental analysis calcd. (%) for $C_{20}H_{48}N_{30}O_{98}Zn_5Si_2W_{24}$: C 3.39, H 0.68, N 5.94, Si 0.79, Zn 4.62, W 62.39; found: C 3.82, H 0.48, N 6.34, Si 0.92, Zn 5.12, W 61.79. IR (cm^{-1}): 3431 (m), 1630 (w), 1539 (w), 1500 (w), 1312 (m), 1071 (w), 957 (s), 785 (s), 620 (s).

$[Cu^I_2Cu^{II}_4(Htrz)_4(trz)_4Cl_2][GeW_{12}O_{40}]\cdot 15H_2O$ (3).

A mixture of $K_8[\gamma\text{-}GeW_{10}O_{36}]\cdot 6H_2O$ (0.434 g, 0.15 mmol), 1,2,4-triazole (0.121 g, 2.0 mmol) and $CuCl_2\cdot 2H_2O$ (0.118 g, 0.65 mmol) was dissolved in 8.0 mL of distilled water. The mixture (pH = 3.02) was then sealed into a 15 mL Teflon-lined autoclave and heated at 180 ºC for 3 days and then cooled down to room temperature at a rate of 10 ºC h^{-1}. Dark blue crystals of **3** were collected and washed with distilled water and dried in air to give the product (yield: 48 % based on Cu). Elemental analysis calcd. (%) for $C_{16}H_{50}N_{24}O_{55}Cl_2Cu_6GeW_{12}$: C 4.59, H 1.20, N 8.02, Ge 1.73, Cu 9.10, Cl 1.69, W 52.66; found: C 4.12, H 1.02 N 8.58, Ge 1.47, Cu 9.53, Cl 1.43, W 53.21. IR (cm^{-1}): 3407 (s), 1622 (m), 1429 (m), 951(s), 874 (m), 783 (w), 659(w).

$[Cu^I_2Cu^{II}_4(Htrz)_4(trz)_4Cl_2][SiW_{12}O_{40}]\cdot 15H_2O$ (4).

A mixture of $K_8[\gamma\text{-}SiW_{10}O_{36}]\cdot 12H_2O$ (0.354 g, 0.12 mmol), 1,2,4-triazole (0.121 g, 2.0 mmol) and $CuCl_2\cdot 2H_2O$ (0.118 g, 0.65 mmol) was dissolved in 8.0 mL of distilled water. The mixture was then sealed into a 15 mL Teflon-lined autoclave and heated at 180 ºC for 3 days and then cooled down to room temperature at a rate of 10 ºC h^{-1}. Dark blue crystals of **4** were collected and washed with distilled water and dried in air to give the product (yield: 43 % based on Cu). Elemental analysis calcd. (%) for $C_{16}H_{50}N_{24}O_{55}Cl_2Cu_6SiW_{12}$: C 4.64, H 1.22, N 8.11, Si 0.68, Cu 9.20, Cl 1.71, W 53.22; found: C 4.22, H 1.68, N 8.58, Si 0.94, Cu 9.53, Cl 1.43, W 52.91. IR (cm^{-1}): 3419 (s), 1645 (m), 1428 (m), 968(s), 867 (m), 796 (w), 647(w).

$K_2Na_2(H_2O)_2[Co_{11}(trz)_{14}(H_2O)_{14}][P_2W_{18}O_{62}]_2\cdot 29H_2O$ (5).

A mixture of $K_6[\alpha\text{-}P_2W_{18}O_{62}]\cdot 15H_2O$ (0.496 g, 0.1 mmol), 1,2,4-triazole (0.114 g, 1.6 mmol) and $CoCl_2\cdot 6H_2O$ (0.147 g, 0.6 mmol) was dissolved in 8.0 mL of distilled water. The pH value of the mixture was carefully adjusted with 2 M NaOH solution to approximately 4.50 and then sealed into a 15 mL Teflon-lined autoclave and heated at 180 ºC for 3 days and then cooled down to room temperature at a rate of 10 ºC h^{-1}. Pink crystals of **5** were collected and washed with distilled water and dried in air to give the product (yield: 35 % based on Co). Elemental analysis calcd. (%) for $C_{28}H_{118}N_{42}O_{169}P_4Na_2K_2Co_{11}W_{36}$: C 2.99, H 1.06, N 5.22, Na 0.41, P 1.10, K 0.69, Co 5.76, W 58.77; found: C 2.56, H 1.49, N 5.65, Na 0.83, P 0.85, K 1.02, Co 6.12, W 59.15. IR (cm^{-1}):

3433 (s), 1624 (s), 1138 (m), 1077 (m), 930 (w), 788 (w), 662 (w).

$[Cu_{12}(trz)_{10}(Htrz)_2(OH)_4(SO_4)_2(H_2O)_6][P_2W_{18}O_{62}]\cdot 28H_2O$ (6).

A mixture of $K_6[\alpha\text{-}P_2W_{18}O_{62}]\cdot 15H_2O$ (0.256 g, 0.05 mmol), 1,2,4-triazole (0.069 g, 1.0 mmol) and $CuSO_4\cdot 5H_2O$ (0.217 g, 0.8 mmol) was dissolved in 8.0 mL of distilled water. The mixture (pH = 1.84) was then sealed into a 15 mL Teflon-lined autoclave and heated at 180 ºC for 3 days and then cooled down to room temperature at a rate of 10 ºC h^{-1}. Pale blue crystals of **6** were collected and washed with distilled water and dried in air to give the product (yield: 46 % based on Cu). Elemental analysis calcd. (%) for $C_{24}H_{98}N_{36}O_{108}P_2S_2Cu_{12}W_{18}$: C 4.23, H 1.45, N 7.39, P 0.91, S 0.94, Cu 11.19, W 48.54; found: C 3.85, H 1.82, N 7.81, P 1.23, S 1.21, Cu 10.67, W 48.24. IR (cm^{-1}): 3458 (s), 1644 (w), 1538 (w), 1089 (s), 961 (m), 910 (m), 784 (w), 562 (w).

X-ray Crystallography

The suitable single crystal of each compound was glued on a glass fiber. Data collection was performed on a Bruker ApexII CCD diffractometer with Mo Kα (λ = 0.71069 Å) at room temperature. A multiscan correction was applied. The structure was solved by the direct method and refined by full matrix least-squares on F^2 using the SHELXL 97 program.[12] During the refinement of these crystal structures, all non-hydrogen atoms were refined anisotropically. The H atoms on their mother carbon and nitrogen atoms were located in calculated positions. The restrains were used to resolve the ADP and NPD errors of some O, C and N atoms by the "ISOR" and "SIMU" instructions. Moreover, some five-member rings of the organic ligands were also restrained with the "AFIX" and "DELU" commands. Furthermore, compounds **5**−**6** exhibit extra solvent accessible voids in the final refinement, but the residual peaks are too weak to be confirmed as solvent molecules. Thus, the SQUEEZE program[13] was used to further estimate the possible solvent accessible voids and the number of solvent water molecules in the crystal structure. Considering that there exist an amount of disordered solvent molecules in **3** and **4**, the SQUEEZE process has been used to remove the electronic contribution of the unidentified solvents. After the SQUEEZE process, the result implies that 216 for **3** (156 for **4**) removed electrons have been found. When the electron density, TGA, and elemental analysis are taken into account, 15 water molecules are determined. The crystal structure of **5** contains large accessible voids that are large enough to fit potential molecules. Based on charge-balance considerations, elemental analyses, and TGA, 17 water molecules were included in the molecular formula directly. For **6**, 26 water molecules were included in the molecular formula directly. Relevant crystal data and structure refinements of compounds **1**−**6** are summarized in Table 1. Selected bond lengths (Å) and angles (˚) for **1**−**6** are listed in the Supporting Information, Tables S1. Crystallographic data for **1**−**6** have been deposited in the Cambridge Crystallographic Data Center with CCDC reference numbers 1020863-1020868.

Physical Techniques

Powder X-ray diffraction measurement was recorded radiation ranging from 5º to 50º at room temperature on a Siemens D5005 diffractometer with Cu-Kα (λ = 1.5418 Å). IR spectra were recorded in the range 400−4000 cm^{-1} on an Alpha Centaurt FT/IR spectrophotometer using KBr pellets. Thermogravimetric analysis (TGA) were performed on a Perkin-Elmer TGA7 instrument in flowing N_2 with a heating rate of 10 °C·min^{-1}. Diffuse reflectivity was measured from 200 to 800 nm using barium sulfate ($BaSO_4$) as a standard with 100% reflectance on a Varian Cary 500 UV−Vis spectrophotometer. Magnetic susceptibilities were measured on finely grounded single crystal samples (grease restricted) with the use of a Quantum Design SQUID magnetometer MPMS-XL.

Results and discussion

Synthesis

Hydrothermal synthesis has recently proven to be a powerful technique in the preparation of organic-inorganic hybrid materials, because hydrothermal conditions can allow the reaction shift from the thermodynamic to the kinetic so that the equilibrium phases are replaced by structurally more complicated metastable phases.[14] In the process of hydrothermal synthesis, several factors can influence the formation of crystal phases, such as initial reactants, molar ratio, pH value, reaction time, and temperature, *etc*. The subtle changes of each factor may cause great alterations of the assembly process, further impacting on the construction of the structures. In this work, many parallel experiments have proven that the pH value of the reaction is a determining factor for the isolation of the compounds **1**–**6**. Compound **1** could only be obtained in the pH range 2–4. If the pH value of the reaction was higher than 4, only large amounts of unidentified powders were obtained. At pH = 2, a high yield of **1** could be ensured. Similarly, compound **2** was obtained at pH = 3.3. Compound **5** could be synthesized in the pH region between 3.5 and 5. Increasing the pH above 5 resulted in amorphous pink-colored powder. Experimental results revealed that the formation of compounds **1**, **2** and **5** was purely pH dependent. As our continuous exploration, when $K_8[\gamma\text{-}GeW_{10}O_{36}]\cdot 6H_2O$ reacted with $CuCl_2\cdot 2H_2O$ in the presence of 1,2,4-triazole at the pH of 3, **3** was discovered. In a similar process to that used for **3**, but with $K_8[\gamma\text{-}SiW_{10}O_{36}]\cdot 12H_2O$ substituting for $K_8[\gamma\text{-}GeW_{10}O_{36}]\cdot 6H_2O$, compound **4** was consecutively made at pH = 2.8, suggesting that small differences in the shape and size of the polyanions [SiW_{10}] and [GeW_{10}] do not affect on the assembly results of the POM/Cu/trz system. However, when dilacunary Keggin polyoxoanion ([SiW_{10}]/[GeW_{10}]) was displaced by saturated polyoxoanion ([SiW_{12}]/[GeW_{12}]), **3** or **4** could not be formed. Besides, when replacing the Cu^{II} ion with Co^{II}, Fe^{II}, Mn^{II}, Ni^{II}, Zn^{II}, Cd^{II} and Ag^{I} ions, only amorphous powders were obtained. As described above, the inherent essentiality of two dilacunary precursors and the nature of TM cations can affect the formation of crystal phases. Besides, it deserves mention that **3** and **4** are mixed-valent compounds with Cu(II)/Cu(I) oxidation states, even though the starting copper precursor is only in the +2 oxidation state. Such a phenomenon has been observed frequently in the hydrothermal reaction system containing N-donor ligands and Cu^{II} ions.[15] Compound **6** was prepared by reaction of $K_6[\alpha\text{-}P_2W_{18}O_{62}]\cdot 15H_2O$, $CuSO_4\cdot 5H_2O$ and 1,2,4-triazole ligands at the pH of 1.8–3. When $CuSO_4$ was replaced by other Cu^{II} salt, such as $CuCl_2\cdot 2H_2O$, $Cu(CH_3COO)_2\cdot 2H_2O$ and $Cu(NO_3)_2\cdot 3H_2O$, compound **6** could not be afforded, implying that $CuSO_4$ may

serve as an additive or structural directing agent for the formation of **6**. Accordingly, the nature of the Cu^{II} salt is crucial for the isolation of **6**. In summary, the pH of the solution, the nature of the metal salt and the structure of polyoxoanion play important roles in the crystallization of **3**, **4** and **6**.

Table 1 Crystal Data and Structural Refinement Parameters for Compounds **1**–**6**

Compound	1	2	3	4	5	6
Formula	$C_{10}H_{24}N_{15}O_{44.5}$-$Co_2SiW_{12}$	$C_{20}H_{48}N_{30}O_{98}$ $Zn_5Si_2W_{24}$	$C_{16}H_{50}N_{24}O_{55}Cl_2$ Cu_6GeW_{12}	$C_{16}H_{50}N_{24}O_{55}Cl_2$ Cu_6SiW_{12}	$C_{28}H_{118}N_{42}O_{169}P_4$ $Na_2K_2Co_{11}W_{36}$	$C_{24}H_{98}N_{36}O_{108}P_2S_2$-$Cu_{12}W_{18}$
M	3418.40	7072.11	4189.73	4145.23	11261.99	6816.96
Crystal system	monoclinic	triclinic	triclinic	triclinic	monoclinic	monoclinic
Space group	*P*2/n	*P*–1	*P*–1	*P*–1	$P2_1/n$	*C*2/m
a (Å)	10.6100(5)	13.0880(5)	11.5510(5)	11.5350(5)	19.1440(5)	24.8710(2)
b (Å)	11.8040(5)	13.7640(5)	12.1300(5)	12.0910(5)	23.3880(5)	14.2534(1)
c (Å)	20.6980(5)	15.9630(5)	14.2860(5)	14.3130(5)	22.8600(5)	20.8280(2)
α (°)	90	99.833(5)	94.156(5)	94.051(5)	90	90
β (°)	102.821(5)	99.520(5)	105.714(5)	105.611(5)	102.838(5)	125.026(3)
γ (°)	90	101.798(5)	106.035(5)	105.770(5)	90	90
V (Å^3)	2527.60(3)	2713.05(5)	1828.27(5)	1827.83(14)	9979.5(4)	6046.25(2)
Z	2	1	1	1	2	4
D_{calc} (mg m^{-3})	4.48	4.32	3.81	3.77	3.63	3.75
μ (mm^{-1})	27.963	26.551	21.085	20.703	21.720	19.298
T (K)	293	293	293	293	293	293
Reflections collected/ unique	12249/4456	14228/9447	10121/6403	10539/6404	50922/17384	17372/5513
GOF	0.967	1.003	1.034	1.029	1.071	1.064
R_1/wR_2 [$I > 2\sigma(I)$]	0.048/0.092	0.057/0.116	0.069/0.159	0.069/0.170	0.068/0.154	0.054/0.144
R_1/wR_2 (all data)	0.089/0.106	0.106/0.140	0.116/0.204	0.091/0.186	0.090/0.170	0.084/0.165

Crystal structure of 1

Single crystal X-ray diffraction analysis reveals that compound **1** crystallizes in the monoclinic, space group *P*2/n; the relevant crystal data and structural refinement parameters are presented in Table 1. As shown in Fig. 1a, **1** consists of two Co atoms, five Htrz ligands, one $[SiW_{12}O_{40}]^{4-}$ cluster, and four point five water molecules. In $[SiW_{12}O_{40}]^{4-}$ anion, the Si1 atom lies on an inversion centre and the central four μ_4 oxygen atoms are observed to be disordered over eight positions with each oxygen site half-occupied. This structure feature of disorder often appears in the Keggin structure, which has been explained in previous literatures.[16] The Si–O bonds range from 1.566(9) to 1.682(9) Å (mean value 1.615 Å). While the W–O distances can be grouped into three sets: W–O_t (terminal) 1.620(1)–1.698(2) Å, W–O_c (central) 2.306(5)–2.476(9) Å, and W–O_b (bridge) 1.838(0)–1.939(1) Å. The crystallographically independent Co1 exhibits a slightly distorted octahedral coordination geometry, defined by four N atoms from four Htrz ligands, one terminal O atom from $[SiW_{12}O_{40}]^{4-}$ and one O atom from water molecule (Co–O 2.166(2) Å, Co–O_w 2.131(6) Å, Co–N 2.066(9)–2.135(9) Å). All the bond lengths are within the normal ranges. In **1**, Htrz ligands exhibit two different coordination modes: three of them serve as bridging ligands in a common N1, N2 mode to links with two Co1, one of which lies about a twofold access (with N5 on the twofold axis); the others only conjugate with Co1 by means of one N atom, resulting in the metal-organic motif $[Co_2(Htrz)_5]^{4+}$. The complexes $[Co_2(Htrz)_5]^{4+}$ and the $[SiW_{12}O_{40}]^{4-}$ anions are alternatively arranged into a 1D zigzag chain (Fig. 1b). The adjacent 1D chains are connected by N–H···O hydrogen bonding interactions between the molecular sheets (Fig. 1c), which are further extended into a 3D supramolecular framework by hydrogen bonding interactions (Fig. S1). The bond valence sum calculations confirm that all W centers are in +6 oxidation states, the Si center is in +4 oxidation state, and the Co center is in +2 oxidation state.[17]

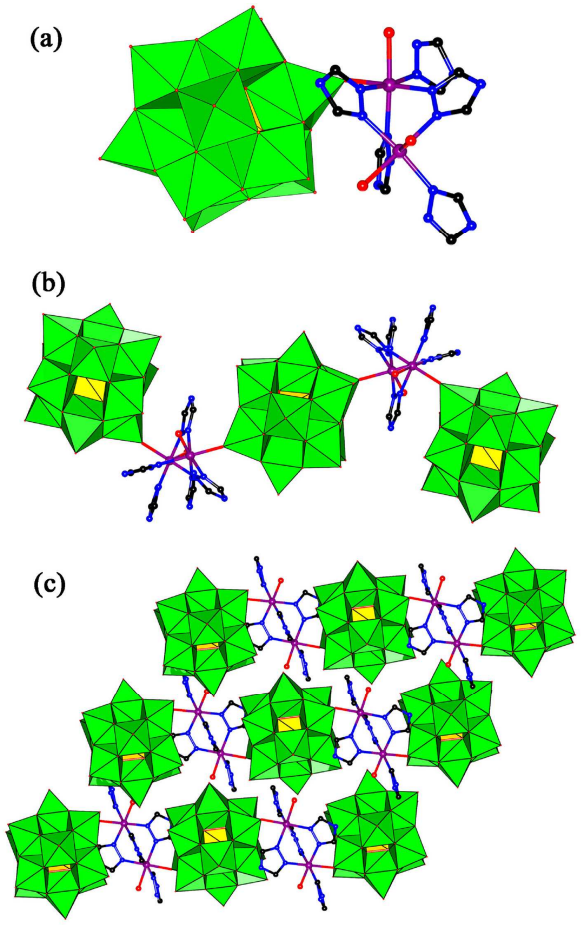

Fig. 1 Crystal structure of **1**: (a) Coordination environment of the Co ions and $[SiW_{12}O_{40}]^{4-}$ anion; (b) 1D zigzag chain of **1** containing the alternative $[Co_2(Htrz)_5]^{4+}$ subunits and $[SiW_{12}O_{40}]^{4-}$ clusters; (c) 2D supramolecular sheet formed by the hydrogen bonding interactions. Color legend: black, C; blue, N; red, O; violet, Co; canary, polyhedron, SiO_4; green polyhedron, WO_6.

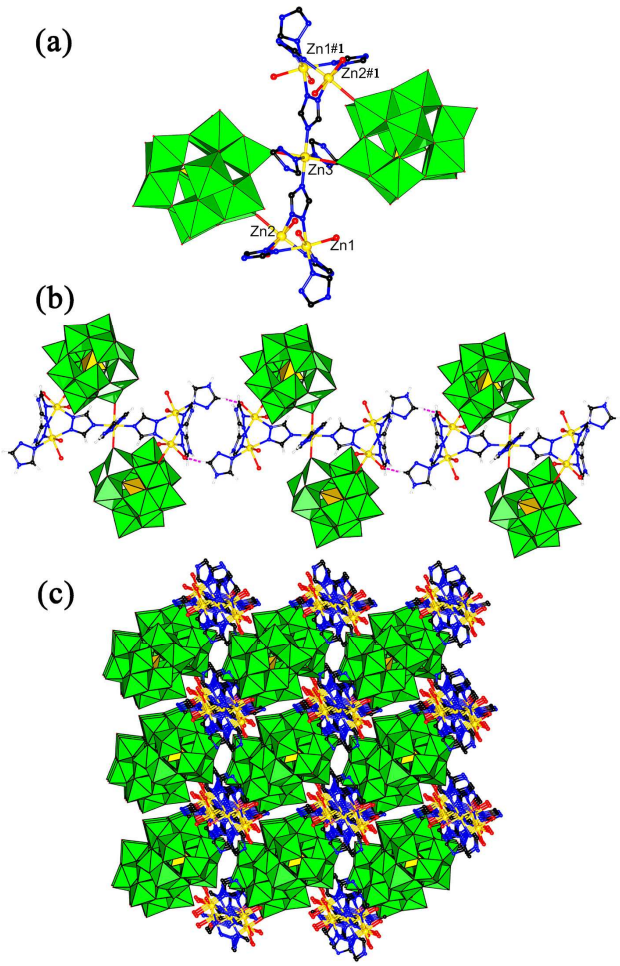

Fig. 2 Crystal structure of **2**: (a) Coordination environment of the Zn ions and $[SiW_{12}O_{40}]^{4-}$ anion; (b) 1D chain formed by the hydrogen bonding interactions; (c) The 3D supramolecular framework formed by the hydrogen bonding interactions in **2**. Color legend: black, C; blue, N; red, O; yellow, Zn; canary, polyhedron, SiO_4; green polyhedron, WO_6. Symmetry operation: #1 -*x*, 1-*y*, 2-*z*.

Crystal structure of 2

Compound **2** crystallizes in the triclinic space group *P*−1. In the asymmetric unit, there are one $[SiW_{12}O_{40}]^{4-}$ anion, two and a half Zn atom, four Htrz ligands, one trz ligand, four coordinated water molecules and five lattice water molecules. There are three crystallographically independent Zn^{2+} ions (Zn1, Zn2 and Zn3), as shown in Fig. 2. The Zn1 ion is six-coordinated by three nitrogen atoms from three Htrz ligands, one nitrogen atom from trz ligand, and two oxygen atoms from two coordination water molecules, showing distorted octahedron geometry. Zn2 is defined by two nitrogen atoms from two Htrz ligand, one nitrogen atom from trz ligand, one terminal oxygen atom from $[SiW_{12}O_{40}]^{4-}$ anion, and two oxygen atoms from two coordination water molecules. The Zn3 atom lies on an inversion centre, which is coordinated by two nitrogen atoms from two Htrz ligands, two nitrogen atoms of two trz ligands and two terminal oxygen atoms from two $[SiW_{12}O_{40}]^{4-}$ anions. Zn1 and Zn2 are linked together by two Htrz ligands through N1, N2-bridging mode, giving rise to $[Zn_2(Htrz)_3]^{4+}$ motif. Two $[Zn_2(Htrz)_3]^{4+}$ units are further connected by Zn3 ion and two trz ligands to give a $[Zn_5(trz)_2(Htrz)_8]^{8+}$ subunit. Each $[SiW_{12}O_{40}]^{4-}$ anion provides two terminal O atoms to link $[Zn_5(trz)_2(Htrz)_8]^{8+}$ motif forming $[Zn_5(trz)_2(Htrz)_8][SiW_{12}O_{40}]_2$ dimer. The $[Zn_5(trz)_2(Htrz)_8][SiW_{12}O_{40}]_2$ dimers are alternatively arranged into a 1D chain by C(8)–H(8)···O(9W) hydrogen bonding interactions (Fig. 2b). The adjacent 1D chains are further extended into a 3D suparmolecular framework through the hydrogen bonding interactions (Fig. 2c).

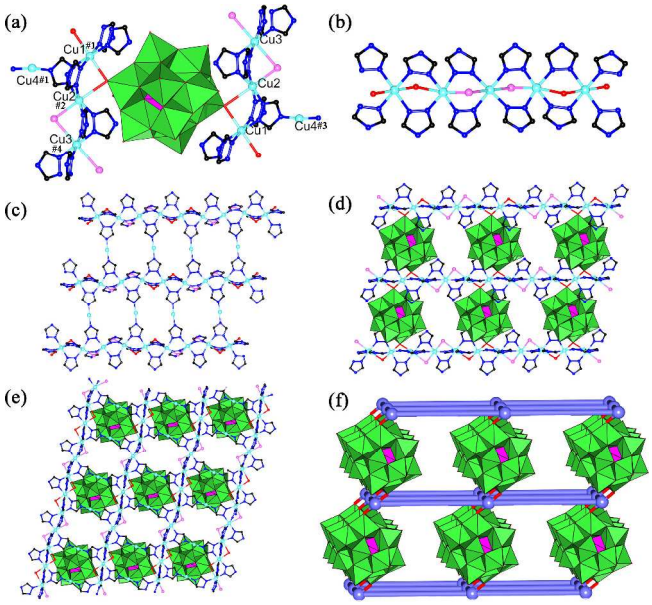

Fig. 3 (a) Ball/stick and polyhedral view of the coordination environment of GeW_{12} polyoxoanion and Cu ions in **3**; (b) View of the 1D organic-inorganic hybrid chain constructed from Cu ions and trz ligands; (c) View of the 2D layer in **3**; (d) The 3D framework of **3** showing 1D channels: along *a* axis and (e) along *b* axis; (f) The topological of 3D cpu network. Color legend: black, C; blue, N; red, O; pink, Cl; turquoise, Cu; lavender polyhedron, GeO_4; green polyhedron, WO_6. Symmetry operation: #1 -1+*x*, -1+*y*, *z*; #2 –*x*, 1-*y*, 2-*z*; #3 1-*x*, 2-*y*, 2-*z*; #4 -1+*x*, -1+*y*, -1+*z*.

Crystal structure of 3 and 4

Taking into account that compounds **3** and **4** are isostructural with only slight differences in bond lengths and bond angles, thus **3** is described as a representative. Single-Crystal X-ray diffraction analysis exhibits that **3** contains a new bi-supporting cluster based on the $[GeW_{12}O_{40}]^{4-}$ (shortened as GeW_{12}) anion (Fig. 3a). Compound **3** crystallizes in the triclinic space group *P*−1, consequently the two supporting equivalent metal-organic fragments $[Cu^{II}_2Cu^{I}(Htrz)_2(trz)_2Cl]^{2+}$ are inter-related by the inversion centre of the Ge atom. The GeW_{12} anion exhibits a distorted α-Keggin configuration. In GeW_{12} anion, the Ge1 atom lies on an inversion centre and the central four μ_4 oxygen atoms are observed to be disordered over eight positions with each oxygen site half-occupied. In compound **3**, there are four crystallographically independent Cu ions exhibiting two kinds of coordination geometries. The Cu1 atom lying on an inversion centre, is bound by four N atoms from two Htrz ligands and two trz ligands (Cu–N 2.047(5) Å), and two equator-positioned terminal O atoms (Cu–O 2.419(9) Å) from GeW_{12} anion. The Cu2 atom is surrounded by four N atoms from two Htrz ligands and two trz ligands, one Cl atom, and one equator-positioned

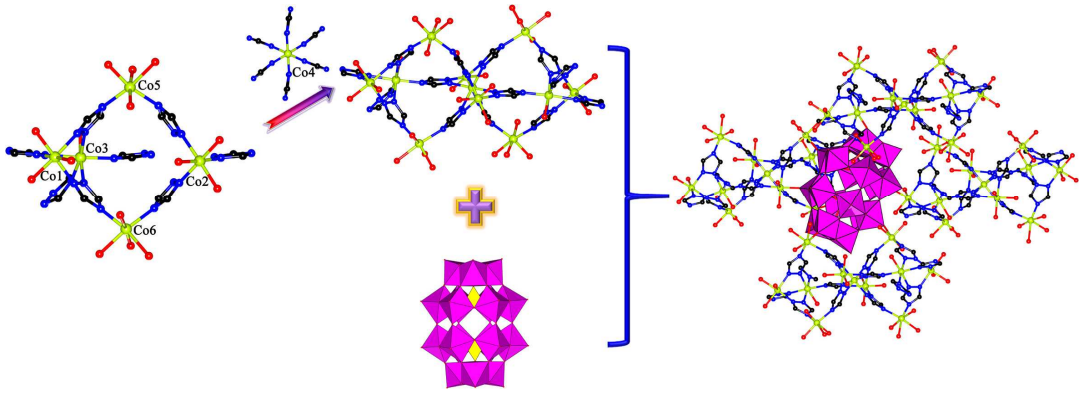

Fig. 4 Structural representations of **5**. Color legend: black, C; blue, N; red, O; lime, Co; purple, W; yellow P.

terminal O atom from GeW_{12} cluster, showing a distorted octahedral coordination geometry (Cu–N 1.987(8) Å, Cu–O 2.739(1) Å, Cu–Cl 2.547(3) Å). The Cu3 atom lies on an inversion centre and has a distorted octahedral geometry, which is coordinated by four N atoms from two Htrz ligands and two trz ligands (Cu–N 1.998(4) Å), and two Cl atoms (Cu–Cl 2.809(5) Å). The Cu4 center adopts an unsaturated linear coordinated mode and is defined by two N atoms from two trz ligands with an average Cu–N distance of 1.861(9) Å. As shown in Fig. 3b, Cu2 links Cu1 and Cu3 together by four trz ligands, resembling an infinite 1D chain. The adjacent 1D chains are linked through N(10)–Cu(4)–N(11) in an opposite direction to form a 2D wall-like layer along the *ac* plane (Fig. 3c). These 2D sheets are further stacked in a parallel fashion through the interactions between GeW_{12} and the copper(II) centers generating a neutral 3D network (Fig. 3d−f) with two types of 1D channels. These channels intersect with each other and run along two different directions: 9.4 × 5.5 $Å^2$ along *a* axis and 8.9 × 6.8 $Å^2$ along *b* axis, as shown in Fig. 3d−e. The channels are occupied by water molecules. A significant aspect in the structure of **3** is that there exists the mixed-valence copper complex, which may become new fascinating materials due to their combined physical properties of Cu^{I} and Cu^{II} ions.[18]

Crystal structure of 5

Compound **5** crystallizes in the monoclinic space group *P*2/n. As shown in Fig. 4, the structure of **5** contains two kinds of motifs: P_2W_{18} polyanions and $[Co_{11}(trz)_{14}(H_2O)_{14}]^{8+}$ cations. The P_2W_{18} polyoxoanion in **5** retains a classical Wells-Dawson structure, which contains two $[\alpha\text{-A-}PW_9O_{34}]^{9-}$ units originating from the α-Keggin polyoxoanion by removal of a suite of three corner-shared WO_6 octahedras. The P–O and W–O lengths are in the normal ranges. The $[Co_{11}(trz)_{14}(H_2O)_{14}]^{8+}$ subunit is built from two $[Co_5]$ fragments and a central $[CoN_6]$ octahedron. The $[Co_5]$ fragment is composed of one $\{Co_2\}$ dimer and one $\{Co_3\}$ triad, which are linked together by two trz ligands (Fig. S2). Co1 is coordinated by three N atoms from three trz ligands, two O atoms from two P_2W_{18} anions and one water molecule. Co3 exhibits the six-coordination environment with five N atoms derived from five trz ligands and one terminal O atom of P_2W_{18} anion. Co1 and Co3 are linked together by three trz ligands, giving rise to a $\{Co_2\}$ dimer. Co2 is defined by three N atoms from three trz ligands, one terminal O atom from P_2W_{18} anion, and two water molecules. Co5 is coordinated by two N atoms from two trz ligands, two terminal O atoms from two P_2W_{18} anions, and two O atoms of water molecules. Co6 is in the octahedral coordination sphere, bonded to two N atoms from two trz ligands, and four O atoms which stem from two P_2W_{18} anions and two water molecules. Co5 and Co6 are linked together through two trz ligands from $[Co2N_3O_3]$ octahedron, resulting into a $\{Co_3\}$ triad. Co4 center, lying on an inversion centre, bonds to six N atoms from six trz ligands, which bridges two adjacent $[Co_5]$ units, generating $[Co_{11}(trz)_{14}(H_2O)_{14}]^{8+}$ unit (Fig. 5a). The P_2W_{18} cluster acts as an octadentate inorganic ligand coordinating with four $[Co_{11}(trz)_{14}(H_2O)_{14}]^{8+}$ motifs through eight terminal O atoms (Fig. S3), while the $[Co_{11}(trz)_{14}(H_2O)_{14}]^{8+}$ fragments act as bridging groups linking eight adjacent P_2W_{18} anions (Fig. 5b), thereby forming the 3D architecture (Fig. 5c). To comprehend the structure better, the 3D structure can be rationalized as a (4, 8) connecting flu (fluorite) network with point symbol $\{4^{12}\cdot6^{12}\cdot8^4\}\{4^6\}_2$, if we assign the P_2W_{18} cluster as a 4-connected node and the $[Co_{11}(trz)_{14}(H_2O)_{14}]^{8+}$ subunit as 8-connected node. An interesting structural feature of compound **5** is that the P_2W_{18} polyanion acts as a ten-dentate inorganic ligand, providing seven terminal oxygen atoms in the equatorial plane and three terminal oxygen atoms in the axial position. Notably, this uncommon coordination pattern of P_2W_{18} polyanion is still relatively scarce, which facilitates the formation of the high-connectivity Wells-Dawson POMs. To our knowledge, **5** contains the largest-ever number of cobalt ions in the $\{P_2W_{18}\}$-based inorganic-organic hybrids.

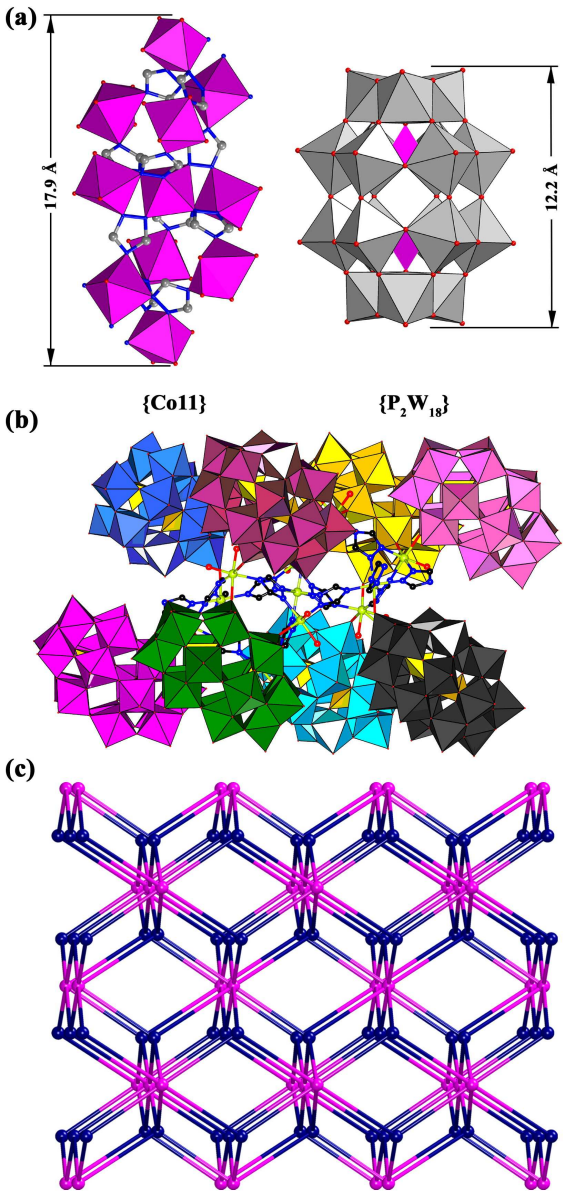

Fig. 5 (a) Polyhedral representations of $\{Co_{11}\}$ and $\{P_2W_{18}\}$ for comparison; (b) The coordination mode of $[Co_{11}(trz)_{14}(H_2O)_{14}]^{8+}$ motif in **5**; (c) The topological of 3D flu network. Color legend: black, C; blue, N; red, O; lime, Co; purple, W; yellow P.

Crystal structure of 6

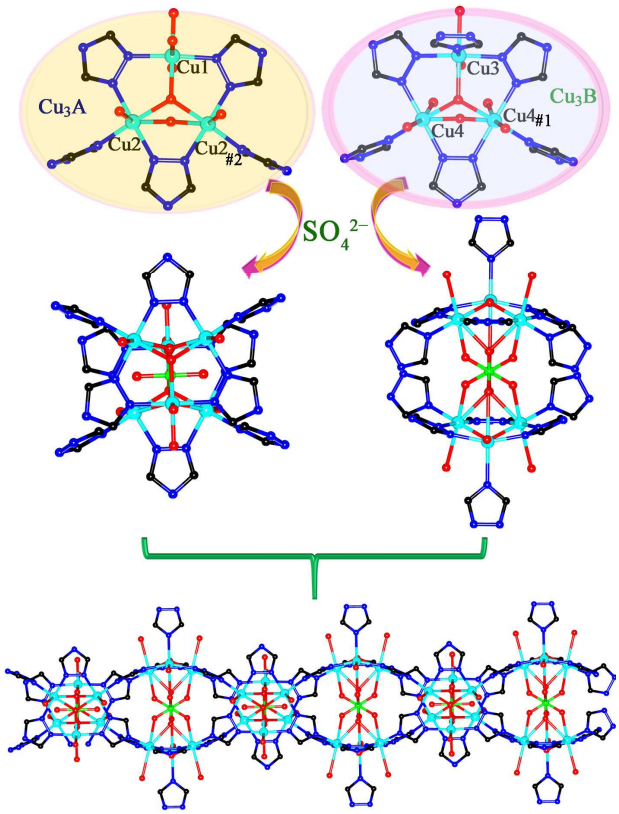

Fig. 6 Stick view of triangular Cu3-triad units, Cu6 hexamers and 1D chain in **6**. Color legend: black, C; blue, N; red, O; turquoise, Cu; green, S. Symmetry operation: #1 *x*, 1-*y*, *z*; #2 *x*, -*y*, *z*.

Compound **6** crystallizes in the monoclinic space group *C*2/m. The single crystal X-ray diffraction analyses reveals that the structure of **6** contains two kinds of motifs: P_2W_{18} polyanions and $[Cu_{12}(trz)_{10}(Htrz)_2(OH)_4(SO_4)_2(H_2O)_6]^{6+}$ cations. These crystals have the crystallographically imposed symmetry disorder, in which S1 and S2 are at sites with 2/m imposed symmetry while P1 lies on twofold axis. There are four independent copper atoms. Cu1 ion sitting on a mirror plane, is defined by two N atoms from two trz ligands, one μ_3-O atom, one O atom from SO_4^{2-} and two O atoms from aqua ligands. Cu2 is coordinated by three N atoms from three trz ligands, one μ_3-O atom and one O atom from SO_4^{2-} as well as one O atom from P_2W_{18} anion, resulting in a distorted octahedral geometry. The Cu3 atom lies on a mirror plane, which is in the octahedral coordination sphere, bonded to three N atoms from three trz ligands, one μ_3-O atom and two O atoms which stem from SO_4^{2-} anions and water molecules. Cu4 ion has the same coordination environment as the Cu2 ion. It should be pointed out that two triangular trinuclear copper units are formed in compound **6**, namely, $[Cu_3(trz)_3(OH)(H_2O)_2]^{2+}$ (abbreviated as Cu_3A) and $[Cu_3(trz)_2(Htrz)(OH)(H_2O)]^{3+}$ (abbreviated as Cu_3B). In the triangular Cu^{II} subunits, three copper cations (Cu2, Cu1, Cu2 or Cu4, Cu3, Cu4) are linked with three trz ligands in a pyrazole-like fashion and bridged by one central μ_3-O atom, as shown in Fig. 6. The identical Cu_3-triad units are joined togetherthrough sharing the center SO_4^{2-} anions, leading to Cu_6 hexamers, $\{[Cu_3(trz)_3(OH)(H_2O)_2]_2SO_4\}^{2+}$ (simplified as Cu_6A) for Cu_3A and $\{[Cu_3(trz)_2(Htrz)(OH)(H_2O)]_2SO_4\}^{4+}$ (simplified as Cu_6B) for Cu_3B, respectively. Interestingly, the Cu_6A and Cu_6B

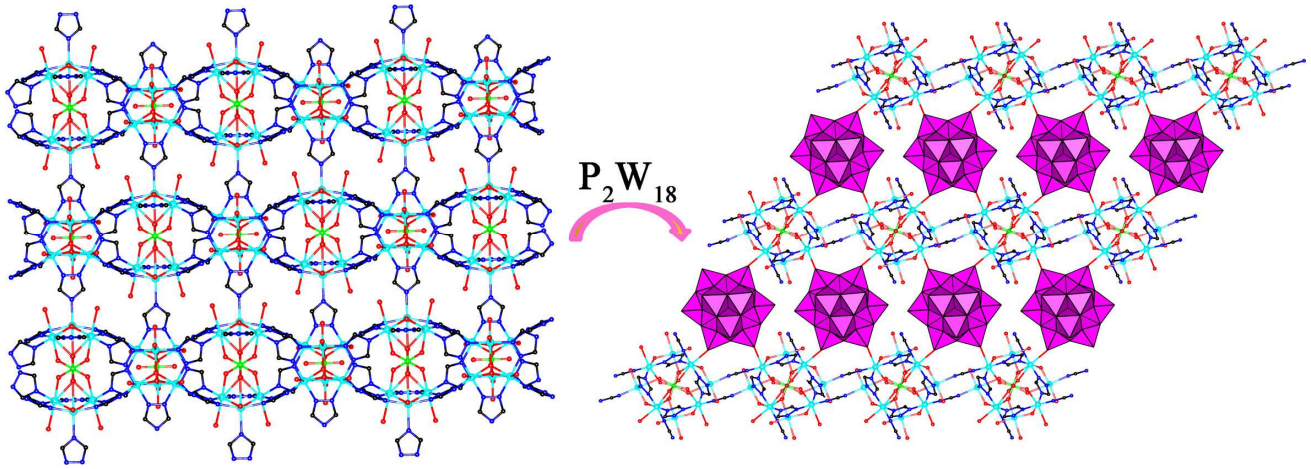

Fig. 7 View of the 2D ladder network (left) constructed from Cu_3-triad and the 3D framework (right) built by P_2W_{18} anions and Cu-trz layers in **6**. Color legend: black, C; blue, N; red, O; turquoise, Cu; green, S; purple, W; yellow P.

segments are connected in an orthogonal fashion by means of owning four trz ligands jointly, consequently forming into a unique 1D chain (Fig. 6). The adjacent chains are interlinked by Cu3 of the triangular units Cu_3B and the third vertex (N10) of the triangular units Cu_3A, resulting in a 2D ladder layer. In addition, each P_2W_{18} polyanion is covalently bonded to four $\{Cu_{12}\}$ units from two adjacent layers, and each $\{Cu_{12}\}$ segment is connected with four P_2W_{18} anions, constructing a beautiful 3D framework (Fig. 7). It is noteworthy that P_2W_{18} anion acts as an eight-dentate inorganic ligand *via* offering eight terminal O atoms in the equatorial plane, which plays an important role in forming the 3D architecture. Besides, in the absence of SO_4^{2-}, the expected compound could not be afforded. In this aspect, undoubtedly, SO_4^{2-} anion as the connector provides a great benefit for aggregating the Cu_3-triads into the larger moieties and further generating the novel 3D structure. Up to now, the largest metal cluster linked by organic amine ligands in POM-based compounds is the nonanuclear subunit from $\{Cu_9(2\text{-ptz})_{12}(H_2O)_6(PMo_{12}O_{40})_2\}\cdot H_2O$.[4] To our knowledge, compound **6** represents the maximum copper cluster linked by amines in the POMs system.

Powder X-ray Diffraction Characterization

Powder X-ray diffraction measurements for **1**−**6** were determined at room temperature (Fig. S4), and the diffraction peak positions of the experimental XRD patterns of **1**−**6** are in agreement with those of simulated XRD patterns, which indicate the phase purity of the samples. The differences in reflection intensity are probably due to preferred orientation in the powder samples.

Thermal Analysis

To characterize the compounds more fully in terms of thermal stability, their thermal behaviors were studied by TGA. The thermal gravimetric analysis was performed under N_2 atmosphere with a heating rate of 10 °C·min^{-1} in the temperature range 50–800 °C, and shown in Fig. S5–10. The TG curve of **1** exhibits three weight loss steps. The first weight loss of 1.58% (calcd 2.14%) below 200 °C can be attributed to the loss of three lattice water molecules. The second weigh loss of 1.05% (calcd 1.46%) in the temperature range of 200–340 °C is assigned to the loss of two coordinated water. In the range of 340–660 °C, the weight loss of 10.84% (calcd 10.07%) corresponds to the decomposition of five Htrz ligands. The TG curve of **2** is similar to that of **1**; first it gradually loses ten lattice water molecules (exptl, 3.36%; calcd, 2.54%) from 50 to 200 °C. On further heating, the materials loses weight continuously during the second step with a weight loss of 2.66% (calcd, 2.03%) from 200 to 370 °C, due to the removal of eight coordinated water molecules. Above 370 °C, the whole framework collapses with the release of ten Htrz ligands (exptl, 9.74%; calcd, 10.54%). Compounds **3** and **4** exhibit the similar weight loss steps. The water molecules are released (50–380 °C for **3**, and 50–400 °C for **4**) with the weight loss of 6.98 % (calcd: 6.45%) for **3**, and 6.14 % (calcd: 6.52%) for **4**. Htrz ligands decompose (380–540 °C for **3,** and 400–560 °C for **4**) with the weight loss of 13.34 % (calcd: 13.19%) for **3**, and 13.72 % (calcd: 13.33%) for **4**, followed by the decomposition of the polyoxoanion. The TG curve of compound **5** indicates that water molecules are eliminated from the network (calcd. 7.41%; found 7.55%) when the temperature is increased from 50 to about 400 °C, after which the removal of the organic components occurred (calcd. 8.85%; found 9.55%). For **6**, TGA curve shows two weight loss processes: the first one (10.41 %) from 50 to 380 °C is equivalent to the loss of 38 water molecules (calcd. 10.03%); the other (11.89%) from 380 to 550 °C corresponds to the loss of twelve Htrz ligands (calcd. 12.16%). The products of the thermal decomposition are amorphous and not further characterized. The observed experimental values are in good agreement with the elemental analyses and the results of single-crystal X-ray structural analyses.

Electrochemistry

As well known, POM have the capacity to deliver the electrons to other species, thus undergoing reversible multi-electron redox process. Consequently, POM can be utilized as the chemically bulk-modified carbon paste electrodes (CPEs) to investigate the electrochemical nature with advantages in many aspects: inexpensive, easy to handle, and easy to prepare.[18a,19] Compounds **1**–**6** are hydrothermally obtained and have low solubility in water

and common organic solvents. The electrochemical behaviors of the compounds **1**–**4** are similar, and the electrochemical behaviors of the compounds **5**–**6** are also homologous. Thus, the **3**-CPE and **6**-CPE cases have been taken as examples to study their electrochemical properties.

For **3**-CPE, in the given range of −650 to +200 mV (Fig. S11), there exist three reversible redox peaks (scan rate: 150 mV s^{-1}) with half-wave potentials at −498 mV (I−I′), −358 mV (II−II′), −199 mV (III−III′) (*vs.* Ag/AgCl), respectively, which can be attributed to the redox of W^{VI} centers of the GeW_{12} polyanion. In addition, an additional quasi-reversible anodic peak (IV) located at +60 mV and the corresponding cathodic peak (−35 mV) is assigned to the redox processes of Cu centers.

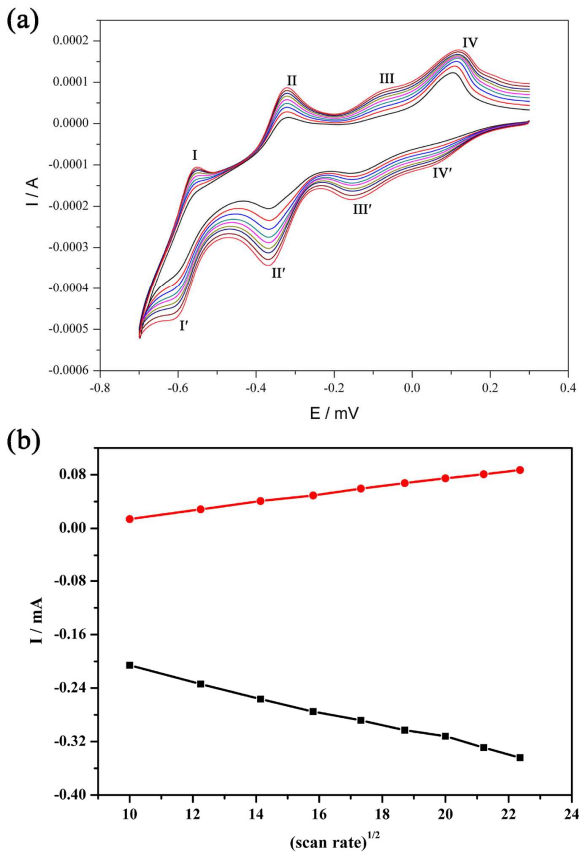

Fig. 8 (a) Cyclic voltammograms of **6** in the potential region of +0.3 to −0.7 V at scan rates (from inner to outer) 100, 150, 200, 250, 300, 350, 400, 450 and 500 mV s^{-1}; (b) the plots of the anodic and the peak (II−II′) currents against the square root of the scan rate.

The cyclic voltammograms for **6**-CPE in a 1 M H_2SO_4 aqueous solution at different scan rates in the potential range of −700 to +300 mV are presented in Fig. 8. The peak potentials change gradually following the scan rates from 100 to 500 mV s^{-1}. The cathodic peak potentials shift toward the negative direction, and the corresponding anodic peak potentials shift to the positive direction along with increasing the scan rates. As seen, the $E_{1/2}$ peak potentials were located at –596 mV, –345 mV and –122 mV (scan rate: 150 mV s^{-1}), respectively, which correspond to the redox of P_2W_{18} polyanion. The fourth reduction wave located at +61 mV and the corresponding oxidation process (+113 mV) is attributed to the redox processes of the Cu centers.[20] As expected, the W^{VI}-based wave is located at a more negative potential than that attributable to the Cu center. The peak (II−II′) currents are proportional to the square root of the scan rate, which suggests that the redox process of **6**-CPE is diffusion-controlled when the scan rate is higher than 100 mV s^{-1}.[21] The electrochemical results indicate that the parent anions maintain its redox ability in the hybrid solids, which can extend the application of these POM-base materials in electrochemistry.

UV–vis absorption spectra and optical band gaps

The UV-vis absorption spectra of three hybrid compounds are presented in Fig. S12. The absorption spectra of compounds **1**–**6** all present one band centered around 270 nm, which is the characteristic band of polyoxometalates assigned as ligand-to-metal charge-transfer (LMCT) transition (O→W).[22] For **1** and **5**, the absorption band in visible region at 500 nm arises from the d-d transition electron transition of Co centers. In the visible light region (at 590 nm), the spectra of the complexes **3**, **4** and **6** present additional bands attributed respectively to the copper centers. The highest occupied molecular orbital (HOMO) and the lowest unoccupied molecular orbital (LUMO) are composed of oxygen 2p and metal d orbitals, respectively. The diffuse reflectance UV–vis spectrum of the powder samples were measured to achieve the HOMO-LUMO gap (*E*), which was determined as the intersection point between the energy axis and the line extrapolated from the linear portion of the adsorption edge in a plot of Kubelka–Munk function $(Fhv)^{0.5}$ against *E* ($F = (1 - R)2/2R$, where R is the reflectance of an infinitely thick layer at a given wavelength).[23] As illustrated in Fig. S13, the corresponding well-defined optical absorption associated with HOMO-LUMO (*E*) can be assessed at 2.72 eV for **1**, 2.82 eV for **2**, 2.28 eV for **3**, 2.34 eV for **4**, 2.41 eV for **5**, 2.84 eV for **6**, which reveals the band gap of the title compounds fall into the range of semiconductor.

Photocatalysis Properties

Recently, photocatalytic properties of POMs have attracted great attention due to their potential applications in purifying water resources. Taking account of water solubility, the typical POM salts may cause the secondary contamination when they are used as photocatalysts to degrade organic dyes. In contrast, POM-based inorganic-organic hybrids display a big potential because of their precious advantages of stability, easily operating, non-secondary-pollution.[20e, 24] In this field, methylene blue (MB), as a model of dye contaminant, is often employed for evaluating the photocatalytic effectiveness in the purification of wastewater.[25]

In this paper, the photocatalytic performance of compounds **5** and **6** were investigated with photodegradation of MB under UV irradiation through a typical process: 50 mg of the compounds was supended into 100 mL of 1.0×10^{-5} mol·L^{-1} MB aqueous solution in a beaker by ultrasonic dispersion for 10 min, magnetically stirred in the dark for about 30 min to ensure the surface-adsorption equilibrium. The mixture was then exposed to UV irradiation from a 125W high pressure Hg lamp and stirred continuously. At given time intervals, 3 mL aliquots were taken out of the beaker, followed by several centrifugations to remove the particles. Then, a clear solution was obtained for UV−vis analysis.

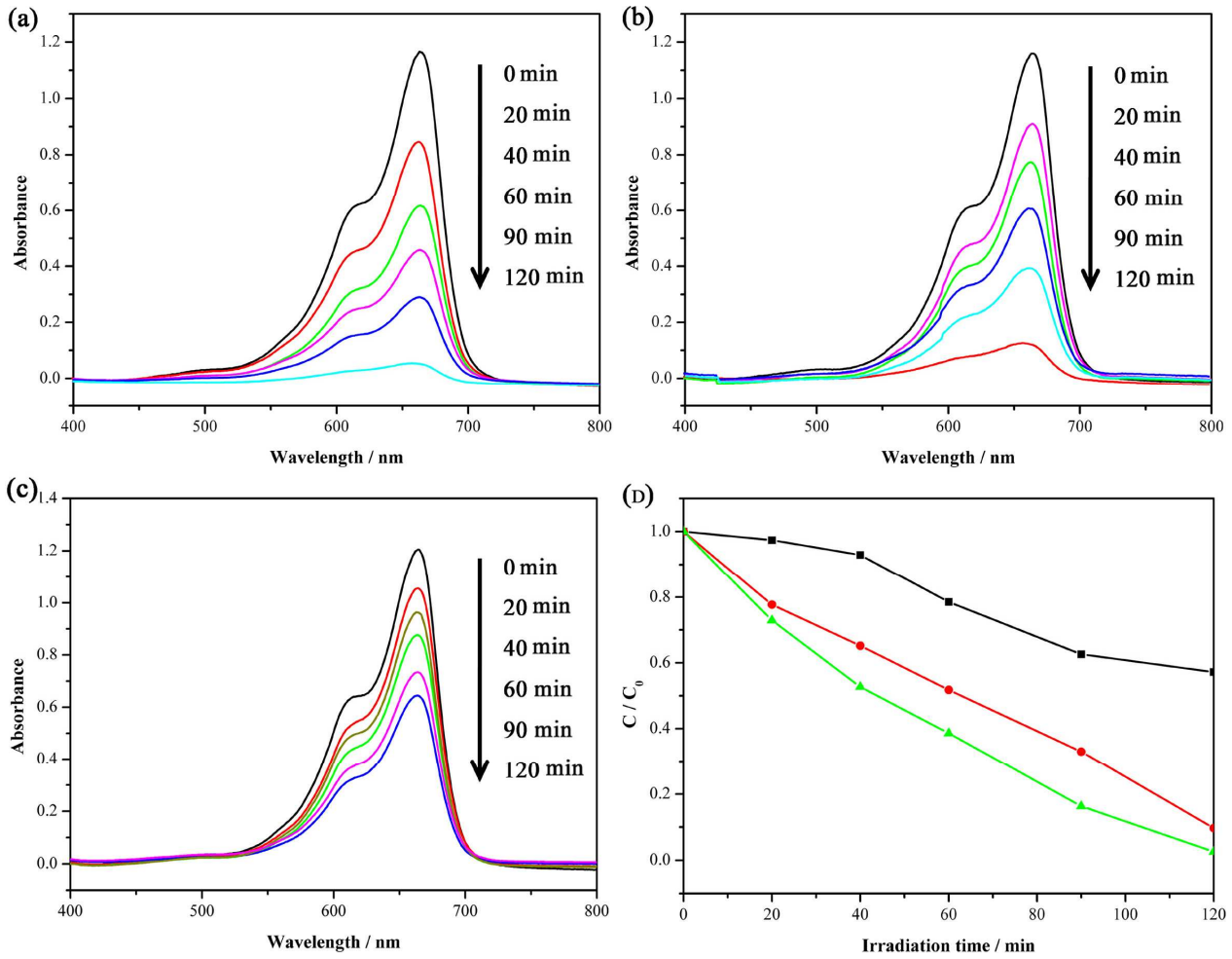

Fig. 9 UV−vis adsorption changes observed for MB solutions as a function of UV light irradiation time: (a) compound **5** as catalyst; (b) compound **6** as catalyst; (c) $(NBu_4)_6[P_2W_{18}O_{62}]$ as catalyst; (d) time dependence MB concentration of **5**, **6** and $(NBu_4)_6[P_2W_{18}O_{62}]$.

The photodegradation of MB assisted by compounds **5**−**6** is shown in Fig. 9a−b. It is obvious that the absorption peak of MB decreased significantly as time goes by. For comparison, insoluble $(NBu_4)_6[P_2W_{18}O_{62}]$ (Fig. 9c) was also employed in the same catalytic experiments. After irradiation for 120 min, the photocatalytic decomposition rates of MB, are 97.3% for **5**, 89.9% for **6**, 42.5% for $(NBu_4)_6[P_2W_{18}O_{62}]$, respectively. Furthermore, the degradation rate curves for compounds **5** and **6** are nearly linear (Fig. 9d). Additionally, the photostabilities of compounds **5** and **6** were monitored by PXRD patterns after the course of the photocatalytic processes. The PXRD patterns are nearly identical to those of the original compounds (Fig. S14). The results indicate that compounds **5** and **6** as stable photocatalysts show outstanding photocatalytic activity for the degradation of MB, which illustrates that the formation of POM-based hybrids could improve the photocatalytic performance. This is probably due to that incorporating transition-metal cations into POMs can increase the valence band position by hybridization of O 2p with d or s orbits of metal cations.[26] As reported, metal-substitution in POMs is a viable route to tune the electronic structure and hence the photochemical reactivity of the cluster.

POMs have similar light absorption and electrochemical band-edge positions to those of TiO_2. Ultraviolet light induce POM to produce oxygen-to-metal charge transfer (OMCT) with promoting electron from the highest occupied molecular orbital (HOMO) to the lowest unoccupied molecular orbital (LUMO). A proposed photodegradation mechanism of organic dyes is deduced: after excited by UV light, *POM is produced, which abstracts electrons from adsorbed water (H_2O_{ads}) molecules and holds the electrons (reaction 1 and 2). The reduced POM (POM^-) is rapidly reoxidized in the presence of O_2 to generate the superoxides (O_2^-) through reaction 3.[27] While, the MB dye is also excited by UV light to generate *MB molecule as reaction 4. Oxidation of the organic reactant occurs via successive attacks by the hydroxyl radicals ($OH^{\cdot}$) and the superoxides (O_2^-) as reaction 5. Finally, after several photo-oxidations, the MB dye is degraded into small molecules. For compounds 5 and 6, the corresponding well-defined optical absorption associated with *Eg* can be assessed at 2.41 and 2.84 eV, respectively. We speculate that the difference performances may originate from the different band gap *Eg,* considering the tests are carried out under the same experiment conditions.

$$POM + h\upsilon \rightarrow {}^{*}POM \quad (1)$$

$$^{*}POM + H_2O \rightarrow POM^{-} + H^{+} + OH^{\bullet} \quad (2)$$

$$POM^{-} + O_2 \rightarrow POM + O_2^{-} \quad (3)$$

$$MB + h\upsilon \rightarrow {}^{*}MB \quad (4)$$

$$^{*}MB + OH^{\bullet} + O_2^{-} \rightarrow \text{degradation products} \quad (5)$$

Magnetic Properties

Magnetic susceptibility data for **1, 3** and **5** were measured in the 2–300 K temperature range with an applied magnetic field of 1000 Oe. Fig. 10a shows the magnetic behavior of compound **1** in the form of $\chi_M T$ versus T and χ_M versus T plots. At room temperature, the experimental $\chi_M T$ value is 5.81 $cm^3 \cdot K \cdot mol^{-1}$ higher than the expected spin-only value ($\chi_M T$ = 3.75 $cm^3 \cdot K \cdot mol^{-1}$, S = 3/2, assuming g = 2) for two high-spin Co(II) atoms in each Co_2 unit per formula, which is caused by an unquenched orbital contribution arising from the $^4T_{1g}$ ground state of Co(II).[28] As the system cools, $\chi_M T$ smoothly decreases over the entire temperature region. In the plot of χ_M versus T, a maximum at 13 K was observed, which suggests the nature of the typical antiferromagnetic interaction between the magnetic centers. In the low-temperature region below 4 K, the increase in the magnetic susceptibility suggests the presence of the paramagnetic impurities in this compound.[28]

For **3**, the observed $\chi_M T$ value of 0.81 $cm^3 \cdot K \cdot mol^{-1}$ at room temperature (Fig. 10b) is smaller than the calculated value of 1.5 $cm^3 \cdot K \cdot mol^{-1}$ for four isolated spin-only Cu^{II} ions for S = 1/2, g = 2.00. With temperature dropping, the value of $\chi_M T$ decreases continuously to a value of of 0.07 $cm^3 \cdot K \cdot mol^{-1}$ at about 2 K, indicating the presence of antiferromagnetic coupling interactions between the Cu^{II} ions.[29]

The magnetic susceptibility of compound **5** was measured in the 2–300 K temperature range under a 1000 Oe applied field. The χ_M slowly increases from 0.12 $cm^3 \cdot mol^{-1}$ at 300 K to 0.44 $cm^3 \cdot mol^{-1}$ at 50 K, and then rapidly reaches the maximum of 2.84 $cm^3 \cdot mol^{-1}$ at 2 K (Fig. 10c). The $\chi_M T$ product is 31.25 $cm^3 \cdot K \cdot mol^{-1}$, being higher than the spin-only value (20.63 $cm^3 \cdot K \cdot mol^{-1}$) for eleven high-spin Co^{2+} ions (S = 3/2, g = 2.0), which illustrates that there is an appreciable spin-orbit coupling expected for octahedral coordinated Co^{2+} ions.[30] Upon cooling, the $\chi_M T$ decreases and attains a minimum of 5.81 $cm^3 \cdot K \cdot mol^{-1}$ at 2 K. This behavior in all probability is indicative of antiferromagentic interactions among Co^{2+} ions.

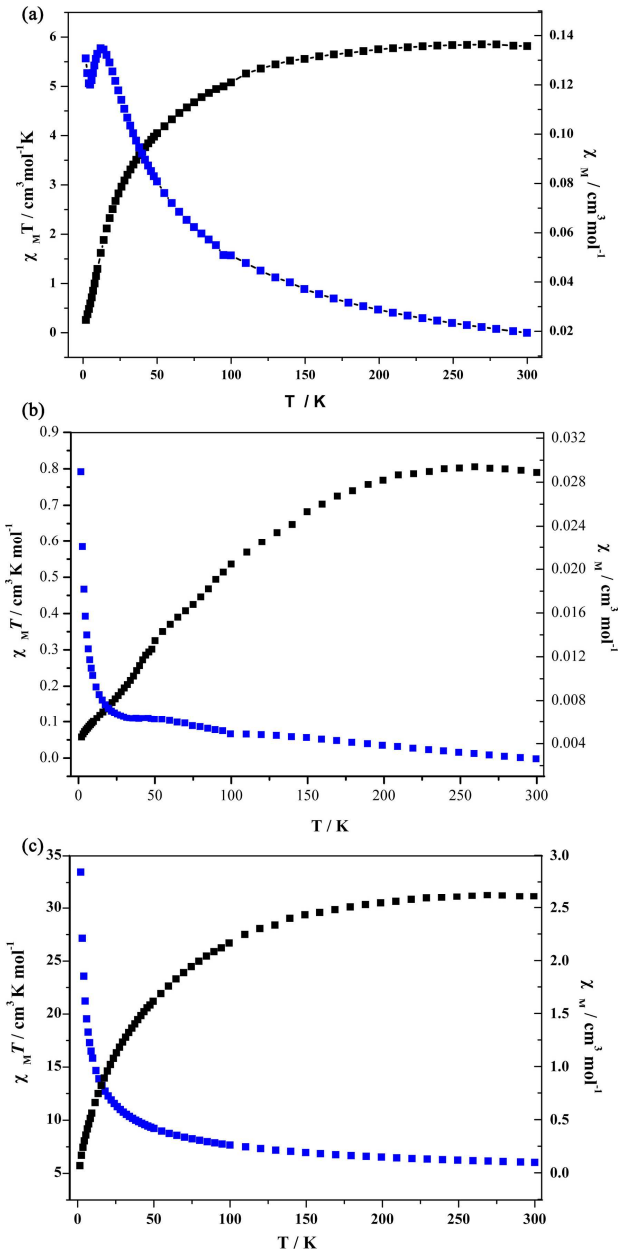

Fig. 10 Plot of temperature dependence of $\chi_M T$ (black square) and χ_M (blue square) versus T for **1** (a), **3** (b), and **5** (c) measured under an applied dc magnetic field of 1000 Oe.

Conclusion

In summary, a family of novel polyoxmetalate-based metal organic framework constructed from polyoxometalate and metal–1,2,4-triazole units have been successfully prepared under hydrothermal conditions, which exhibit 0D dimer, 1D chain and 3D frameworks, respectively. Compound **1** emerges 1D chain build by $[SiW_{12}O_{40}]^{4-}$ anions via dinuclear $[Co_2(Htrz)_5]^{4+}$ bridges, while **2** is a novel dimer constructed from two $[SiW_{12}O_{40}]^{4-}$ linked by $[Zn_5(trz)_2(Htrz)_8]^{8+}$ motif. Compounds **3** and **4** are isostructural three-dimensional frameworks, which are made up from $Cu^{I/II}$–organic sheets and polyanions, possessing two-directional intersecting channels with window dimensions of 9.4 × 5.5 $Å^2$ along the a axis and 8.9 × 6.8 $Å^2$ along the b axis, respectively. Compound **5** contains the largest-ever number of cobalt ions in the $\{P_2W_{18}\}$-based inorganic-organic hybrids. Compound **6** has the characteristic of a triangular Cu-trz unit-based MOF, in which SO_4^{2-} anion as the connector provides a great benefit for generating the novel 3D framework. To the best of our knowledge, **6** represents the maximum copper cluster linked by amine in the POMs system. The preparation of compounds **1**–**6** may reveal a new route to explore novel metal–organic secondary building units based on TM ions and tridentate-bridging ligands by the use of POMs with different types, charges, sizes and shapes so as to construct multifunctional

polyoxoanion-multinuclear transition metal complex hybrid materials with various architectures. In addition, compounds **5** and **6** exhibit remarkable photocatalytic activities for the degradation of MB, which sets a foundation for further development of photocatalysts from other inorganic-organic hybrids based on multinuclear subunits and polyoxometalates.

Acknowledgements

This work was financially supported by the NSFC of China (No. 21471027, 21171033, 21131001, 21222105), National Key Basic Research Program of China (No. 2013CB834802), The Foundation for Author of National Excellent Doctoral Dissertation of P. R. China (FANEDD) (No. 201022), Changbai mountain scholars of Jilin Province and FangWu distinguished young scholar of NENU. We thank three reviewers for their helpful comments.

Notes and references

Institute of Functional Material Chemistry, Key Lab of Polyoxometalate Science of Ministry of Education, Faculty of Chemistry, Northeast Normal University, Changchun 130024, P. R. China. Fax: +86-431-85684009; Tel: +86-431-85099108. E-mail:qinc703@nenu.edu.cn; zmsu@nenu.edu.cn.

† Electronic Supplementary Information (ESI) available: XRPD, TGA, UV-vis absorption spectrum, CV, Table, X-ray crystallographic files in CIF format. See DOI:10.1039/b000000x/

1. (a) M. T. Pope, *Heteropoly and Isopoly Oxometalates*, Springer, Berlin, **1983**. (b) M. T. Pope, *in Comprehensive Coordination Chemistry II* (Eds.: McCleverty, J. A.; Meyer T. J.), Elsevier, Oxford, **2004**. (c) D. L. Long, E. Burkholder, L. Cronin, *Chem. Soc. Rev.* 2007, **36**, 105. (d) Y. Q. Jiao, C. Qin, X. L.Wang, C. G. Wang, C. Y. Sun, H. N. Wang, K. Z. Shao and Z. M. Su, *Chem.–Asian J.* 2014, **9**, 470. (e) W. C. Chao, X. L. Wang, Y. Q. Jiao, P. Huang, E. L. Zhou, Z. M. Su, K. Z. Shao, *Inorg. Chem.* 2014, **53**, 9486.
2. (a) C. L. Hill, C. M. Prosser-McCartha, *Coord. Chem. Rev.* 1995, **143**, 407. (b) A. Proust, R. Thouvenot, P. Gouzerh, *Chem. Commun.* 2008, 1837. (c) K. Suzuki, Y. Kikukawa, S. Uchida, H. Tokoro, K. Imoto, S. Ohkoshi, N. Mizuno, *Angew. Chem. Int. Ed.* 2012, **51**, 1597. (d) C. Lydon, M. M. Sabi, M. D. Symes, D. L. Long, M. Murrie, S. Yoshii, H. Nojiri, L. Cronin, *Chem. Commun.* 2012, **48**, 9819. (e) K. Nakajima, K. Eda, S. Himeno, *Inorg. Chem.* 2010, **49**, 5212. (f) U. Kortz, F. Hussain, M. Reicke, *Angew. Chem. Int. Ed.* 2005, **44**, 3773. (g) M. T. Pope, A. Müller, *Angew. Chem. Int. Ed. Engl.* 1991, **30**, 34. (h) A. Ogata, H. Yanagie, E. Ishikawa, Y. Morishita, S. Mitsui, A. Yamashita, K. Hasumi, S. Takamoto, T. Yamase, M. B. Eriguchi, *J. Cancer.* 2008, **98**, 399. (i) X. K. Fang, M. Sepeldrich, H. Schilder, R. Cao, K. P. O'Halloran, C. L. Hill, P. Kögerler, *Chem. Commun.* 2010**,** **46**, 2760. (j) Y. Q. Jiao, C. Qin, X. L. Wang, F. H. Liu, P. Huang, C. G. Wang, K. Z. Shao, Z. M. Su*, Chem. Commun.* 2014, **50**, 5961.
3. (a) S. Uchida, R. Kawamoto, H. Tagami, Y. Nakagawa, N. Mizuno, *J. Am. Chem. Soc.* 2008, **130**, 12370. (b) F. J. Ma, S. X. Liu, C. Y. Sun, D. D. Liang, G. J. Ren, F. Wei, Y. G. Chen, Z. M. Su, *J. Am. Chem. Soc.* 2011, **133**, 4178.(c) H. Fu, C. Qin, Y. Lu, Z. M. Zhang, Y. G. Li, Z. M. Su, W. L. Li, E. B. Wang, *Angew. Chem. Int. Ed.* 2012, **51**, 7985. (d) Q. X. Han, C. He, M. Zhao, B. Qi, J. Y. Niu, C. Y. Duan, *J. Am. Chem. Soc.* 2013, **135**, 10186. (e) J. W. Zhao, J. L. Zhang, Y. Z. Li, J. Cao, L. J. Chen, *Cryst. Growth Des.* 2014, **14**, 1467.
4. X. Y. Wu, Q. K. Zhang, X. F. Kuang, W. B. Yang, R. M. Yu, C. Z. Lu, *Dalton Trans.* 2012, **41**, 11783.
5. (a) J. Q. Sha, L. Y. Liang, J. W. Sun, A. X. Tian, P. F. Yan, G. M. Li, C. Wang, *Cryst. Growth Des.* 2012, **12**, 894. (b) X. L. Wang, N. Li, A. X. Tian, J. Ying, G. C. Liu, H. Y. Lin, J. W. Zhang, Y. Yang, *Dalton Trans.* 2013, **42**, 14856. (c) X. Wang, M. M. Zhang, X. L. Hao, Y. H. Wang, Y. Wei, F. S. Liang, L. J. Xu, Y. G. Li, *Cryst. Growth Des.* 2013, **13**, 3454. (d) C. Zou, Z. Zhang, X. Xu, Q. Gong, J. Li. C. D. Wu, *J. Am. Chem. Soc.* 2012, **134**, 87.
6. (a) J. P. Zhang, Y. Y. Lin, W. X. Zhang, X. M. Chen, *J. Am. Chem. Soc.* 2005, **127**, 14162. (b) A. X. Tian, J. Ying, J. Peng, J. Q. Sha, Z. G. Han, J. F. Ma, Z. M. Su, N. H. Hu, H. Q. Jia, *Inorg. Chem.* 2008, **47**, 3274. (c) D. D. Wang, J. Peng, P. P. Zhang, X. Wang, M. Zhu, M. G. Liu, C. L. Meng, K. Alimaje, *Inorg. Chem. Commun.* 2011, **14**, 1911. (d) Y. Q. Jiao, C. Qin, C. Y. Sun, K. Z. Shao, P. J. Liu, P. Huang, K. Zhou, Z. M. Su, *Inorg. Chem. Commun.* 2012, **20**, 273.
7. (a) Q. G. Zhai, X. Y. Wu, S. M. Chen, C. Z. Lu, W. B. Yang, *Cryst. Growth Des.* 2006, **6**, 2126. (b) J. P. Zhang, X. M. Chen, *Chem. Commun.* 2006, 1689. (c) Q. G. Zhai, C. Z. Lu, X. Y. Wu, S. R. Battern, *Cryst. Growth Des.* 2007, **7**, 2332. (d) G. Wei, Y. F. Shen, Y. R. Li, X. C. Huang, *Inorg. Chem.* 2010, **49**, 9191.
8. (a) N. Masciocchi, S. Galli, A. Sironi, *Inorg. Chem.* 2005, **26**, 1. (b) J. P. Zhang, Y. B. Zhang, J. B. Lin, X. M. *Chen, Chem. Rev.* 2012, **112**, 1001.
9. X. F. Kuang, X. Y. Wu, R. M. Yu, J. P. Donahue, J. S. Huang, C. Z. Lu, *Nat. Chem.* 2010, **2**, 461.
10. X. F. Kuang, X. Y. Wu, J. Zhang, C. Z. Lu, *Chem. Commun.* 2011, **47**, 4150.
11. (a) J. Canny, A. Tézé, R. Thouvenot, G. Hervé, *Inorg. Chem.* 1985, **25**, 2114. (b) R. Contant, *Inorg. Synth.* 1990, **27**, 104. (c) D. K. Lyon, W. K. Miller, T. Novet, P. J. Domaille, E. Evitt, D. C. Johnson, R. G. Finke, *J. Am. Chem. Soc.* 1991, **113**, 7209. (d) N. H. Nsouli, B. S. Bassil, M. H. Dickman, U. Kortz, B. Keita, L. Nadjo, *Inorg. Chem.* 2006, **45**, 3860. (e) C. R. Graham, R. G. Finke, *Inorg. Chem.* 2008, **47**, 3679.
12. (a) G. M. Sheldrick, *SHELXL97*, *Program for Crystal Structure Refinement*; University of Göttingen: Göttingen, Germany, **1997**. (b) G. M. Sheldrick, *SHELXS97*, *Program for Crystal Structure Solution*; University of Göttingen: Göttingen, Germany, **1997**. (c) G. M. Sheldrick, *Acta Crystallogr. Sect. A* 1990, **46**, 467. (d) G. M. Sheldrick, *Acta Crystallogr. Sect. A* 2008, **64**, 112. (e) L. J. Farrugia, *J. Appl. Crystallogr*. 1999, **32**, 837.
13. (a) A. L. Spek, PLATON, *A Multipurpose Crystallographic Tool*; Utrecht University: Utrecht, The Netherlands, **1998**. (b) A. L. Spek, *Acta Cryst*. 2009, D65, 148.
14. (a) J. Gopalakrishnan, *Chem. Mater.* **1995**, 7, 1265. (b) J. W. Zhao, C. M. Wang, J. Zhang, S. T. Zheng, G. Y. Yang, *Chem.−Eur. J.* 2008, **14**, 9223. (c) J. Y. Niu, S. W. Zhang, H. N. Chen, J. W. Zhao, P. T. Ma, J. P. Wang, *Cryst. Growth Des.* 2011, **11**, 3769. (d) S. W. Zhang, J. W. Zhao, P. T. Ma, H. N. Chen, J. Y. Niu, J. P. Wang, *Cryst. Growth Des.* 2012, **12**, 1263.
15. (a) X. M. Zhang, M. L. Tong, X. M. Chen, *Angew. Chem., Int. Ed.* 2002, **114**, 1071. (b) C. M. Liu, D. Q. Zhang, D. B. Zhu, *Cryst. Growth Des.* 2005, **5**, 1639. (c) M. G. Liu, P. P. Zhang, J. Peng, H. X. Meng, X. Wang, M. Zhu, D. D. Wang, C. L. Meng, K. Alimaje, *Cryst. Growth Des.* 2012, **12**, 1273.
16. (a) Z. G. Han, Y. Z. Gao, X. L. Zhai, J. Peng, A. X. Tian, Y. L. Zhao, C. W. Hu, *Cryst. Growth Des.* 2009, **9**, 1225. (b) W. L. Zhou, J. Liang, C. Qin, K. Z. Shao, F. M. Wang, Z. M. Su, *CrystEngComm* 2014, **16**, 7410.
17. I. D. Brown, D. Altermatt, *Acta Crystallogr. Sect. B* 1985, **41**, 244.
18. (a) Y. Gong, T. Wu, P. G. Jiang, J. H. Lin, Y. X. Yang, *Inorg. Chem.* 2013, **52**, 777. (b) L. J. Dong, X. F. Li, J. Cao, W. Chu, R. D. Huang, *Dalton Trans.* 2013, **42**, 1342.
19. (a) X. L. Wang, J. Li, A. X. Tian, D. Zhao, G. C. Liu, H. Y. Lin, *Cryst. Growth Des.* 2011, **11**, 3456. (b) B. Nohra, H. El-Moll, L. M. Rodriguez-Albelo, P. Mialane, J. Marrot, C. Mellot-Draznieks, M. O'Keeffe, R. N. Biboum, J. Lemaire, B. Keita, L. Nadjo, A. Dolbecq, *J. Am. Chem. Soc.* 2011, **133**, 13363. (c) X. L. Wang, C. Xu, H. Y. Lin, G. C. Liu, S. Yang, Q. Gao, A. X. Tian, *CrystEngComm* 2012, **14**, 5836. (d) M. D. Symes, L. Cronin, *Nat. Chem.* 2013, **5**, 403.
20. (a) B. Keita, I. M. Mbomekalle, L. Nadjo, R. Contant, *Electrochem. Commun.* 2000, **2**, 720. (b) S. Nellutla, J. van Tol, N. S. Dalal, L. H. Bi, U. Kortz, B. Keita, L. Nadjo, G. A. Khitrov, A. G. Marshall, *Inorg. Chem.* 2005, **44**, 9795. (c) C. Pichon, P. Mialane, A. Dolbecq, J. Marrot, E. Rivière, B. Keita, L. Nadjo, F. Sécheresse, *Inorg. Chem.* 2007, **46**, 5292. (d) S. S. Mal, B. S. Bassil, M. Ibrahim, S. Nellutla, J. van Tol, N. S. Dalal, J. A. Fernández, X. López, J. M. Poblet, R. N.

Biboum, B. Keita, U. Kortz, *Inorg. Chem.* 2009, **48**, 11636. (e) H. Fu, Y. G. Li, Y. Lu, W. L. Chen, Q. Wu, J. X. Meng, X. L. Wang, Z. M. Zhang, E. B. Wang, *Cryst. Growth Des.* 2011, **11**, 458.

21. (a) B. S. Bassil, M. Ibrahim, S. S. Mal, A. Suchopar, R. N. Biboum, B. Keita, L. Nadjo, S. Nellutla, J. van Tol, N. S. Dalal, U. Kortz, *Inorg. Chem.* 2010, **49**, 4949. (b) S. G. Mitchell, T. Boyd, N. M. Haralampos, D. L. Long, L. Cronin, *Inorg. Chem.* 2011, **50**, 136.
22. C. Streb, *Dalton Trans.* 2012, **41**, 1651.
23. J. I. Pankove, *Optical Processes in Semiconductors*, Prentice-Hall, Inc., Englewood Cliffs, NJ, **1971**, pp. 34.
24. (a) Q. Wu, W. L. Chen, D. Liu, C. Liang, Y. G. Li, S.W. Lin, E. B. Wang, *Dalton Trans.* 2011, **40**, 56. (b) M. T. Li, J. Q. Sha, X. M. Zong, J. W. Sun, P. F. Yan, L. Li, X. N. Yang, *Cryst. Growth Des.* 2014, **14**, 2794.
25. (a) X. L. Wang, J. J. Cao, G. C. Liu, A. X. Tian, J. Luan, H. Y. Lin, J. W. Zhang, N. Li, *CrystEngComm* 2014, **16**, 5732. (b) X. L. Wang, Z. H. Chang, H. Y. Lin, A. X. Tian, G. C. Liu, J. W. Zhang, *Dalton Trans.* 2014, **43**, 12272.
26. (a) Z. Y. Zhang, Q. P. Lin, S. T. Zheng, X. H. Bu, P. Y. Feng, *Chem. Commun.* 2011, **47**, 3918. (b) J. Tucher, Y. L. Wu, L. C. Nye, I. Ivanovic-Burmazovic, M. M. Khusniyarov, C. Streb, *Dalton Trans.* 2012, **41**, 9938. (c) J. Tucher, L. C. Nye, I. Ivanovic-Burmazovic, A. Notarnicola, C. Streb, *Chem.–Eur. J.* 2012, **18**, 10949.
27. (a) Z. Q. Yu and S. S. C. Chuang, *J. Phys. Chem. C* 2007, **111**, 13813. (b) A. Houas, H. Lachheb, M. Ksibi, E. Elaloui, C. Guillard, J.-M. Herrmann, *Appl. Catal. B-Environ.* 2001, **31**, 145.
28. (a) A. Palii, B. Tsukerblat, S. Klokishner, K. R. Dunbar, J. M. Clemente-Juan, E. Coronado, *Chem. Soc. Rev.* 2011, **40**, 3130. (b) J. M. Clemente-Juan, E. Coronado, A. Gaita-Arino, *Chem. Soc. Rev.* 2012, **41**, 7464. (c) C. Y. Sun, X. J. Zheng, S. Gao, L. C. Li, L. P. Jin, *Eur. J. Inorg. Chem.* 2005, 4150. (d) X. Y. Zhao, D. D. Liang, S. X. Liu, C. Y. Sun, R. G. Cao, C. Y. Gao, Y. H. Ren, Z. M. Su, *Inorg. Chem.* 2008, **47**, 4150. (e) X. B. Li, J. Y. Zhang, Y. Q. Wang, Y. Song, E. Q. Gao, *Chem.−Eur. J.* 2011, **17**, 13883.
29. (a) C. Z. Ruan, R. Wen, M. X. Liang, X. J. Kong, Y. P. Ren, L. S. Long, R. B. Huang, L. S. Zheng, *Inorg. Chem.* 2012, **51**, 7587. (b) H. Y. Zhao, J. W. Zhao, B. F. Yang, H. He, G. Y. Yang, *CrystEngComm* 2013, **15**, 5209. (c) J. Y. Niu, P. T. Ma, H. Y. Niu, J. Li, J. W. Zhao, Y. Song, J. P. Wang, *Chem.–Eur. J.* 2007, **13**, 8739.
30. S. Wang, J. Qin, X. L. Wang, C. Qin, T. T. Li, Z. M. Su, *CrystEngComm* 2011, **13**, 325.